Making Mobile Nanotechnology Accessible: Is the Explicit Preparation of Janus Nanoparticle Necessary to Achieve Mobility?

Vagisha Nidhi , Arthur Allaire , Zakariya Ait Athmane , Patrick Guenoun , Fabienne Testard * , Jean-Philippe Renault * , Florent Malloggi *

Posted Date: 10 September 2024

doi: 10.20944/preprints202409.0820.v1

Keywords: self-propulsion; mobility; chemotaxism; Janus particles; Gold-Silica particles; DLS; PTV

Article

Making Mobile Nanotechnology Accessible: Is the Explicit Preparation of Janus Nanoparticle Necessary to Achieve Mobility?

Vagisha Nidhi, Arthur Allaire, Zakariya Ait Athmane, Patrick Guenoun, Fabienne Testard *, Jean-Philippe Renault * and Florent Malloggi *

Université Paris-Saclay, CEA Saclay, CNRS, NIMBE, UMR 3685, LIONS, 91191 Gif-Sur-Yvette Cedex, France
* Corresponding: jean-philippe.renault@cea.fr, tel +33169081550, Florent.malloggi@cea.fr; or Fabienne.testard@cea.fr

Abstract: This study investigates the necessity of particle asymmetry for self-propulsion in nanomotors. While conventional wisdom posits that asymmetric designs are crucial for generating phoretic forces or localized bubble propulsion, recent research suggests that symmetrical particles may also exhibit motility. To address this debate, we developed a robust workflow for synthesizing gold grafted silica nanoparticles with precise control over size and shape, enabling the direct comparison of their motile behavior by dynamic light scattering and particle tracking velocimetry. Our results indicate that the inherent asymmetry generated during isotropic gold nanoparticle deposition onto silica surfaces may enable particle motility.

Keywords: self-propulsion; mobility; chemotaxism; Janus particles; Gold-Silica particles; DLS; PTV

Introduction

Nano and micro swimmers, nano and microscale devices that are capable of converting various forms of energy into mechanical motion, have garnered significant attention due to their potential applications in targeted drug delivery, nanoscale assembly, environmental sensing and remediation [1]. Since than more a decade, different strategies were used to develop artificial materials inspired by self-propulsed microorganisms or bacterias [2]. Various forms of energy input—chemical, optical, magnetic, or electrical—were used to drive nano or micromotors. Optical propulsion, for example, exploit light-induced forces, such as those arising from plasmonic effects, to achieve movement [3]. While, chemical propulsion usually involves catalytic reactions on the nanomotor's surface [2]. In such case, a fuel source is generally present around the nanomotors. It is currently thought that, if the particle is asymmetric, these catalytic reactions create chemical and/or thermal gradients that generate propulsion through phoretic forces [4,5]. For specific fuel like H_2O_2 that decomposes with gas production, an alternative mechanism is localized bubble propulsion[6]. These considerations have led to the design of nanoswimmers with pronounced asymmetries [7–10]. Thus, Janus particles (made of two different faces) [11] are generally designed to confer asymmetry to isotropic spherical shapes. The requirement of asymmetry is so deeply rooted that, in most of these studies, the non-asymetric particles were not even compared to the asymetric ones. However, some other argue that a perfect asymmetry is not mandatory to obtain motion [12–14]. When a taxis is sought, Janus structure may even be detrimental as it causes poor directionality due to reorientation of the catalytic side. The propulsion then rely on the self-generated concentration field around the colloid [15,16]. It appears that fast asymmetric catalysis doesn't necessarily provide an efficient self-propulsion beyond the Brownian motion [17]. All these observation questions the mechanisms of self-propulsion (self electrophoresis, self diffusion, ..) and the requirement to design an optimized nanomotors. As, obvisously, Janus particles are quite complex to prepare with reproducibility and geometry control it would be of tremendeous interest to obtain motile particles without particular asymmetry.

In this paper, we designed a robust particle preparation workflow allowing to compare exactly the mobility of particles made of similar composition excepted for their asymmetry. The synthetic

 doi:10.20944/preprints202409.0820.v1

pathways were chosen to prepare large amount of particles in a reproducible manner. For such a precise control, gold was preferred to platinum or to catalase, as its nanoparticle preparation are much more controlled and its lower activity minimize bubble production [18]. The changes in diffusion were measured in two conditions, i) in bulk using DLS, and ii) in microfluidic channel, in order to suppress collective effect.

Materials and Methods

Materials

(3-Aminopropyl) triethoxysilane (APTES) 99% (CAS N°: 919-30-2), Hexane (CAS N°: 110-54-3), Paraffin wax (CAS N°: 8002-74-2), Poly-L-lysine (PLL) solution 0.1 % (w/v) in H_2O (CAS N°:25988-63-0), Poly(allylamine hydrochloride) (PAH) M_w ~ 17500 (CAS N°:71550-12-4), Tetraethyl orthosilicate (TEOS) 99.99% (CAS N°: 78-10-4), Sodium chloride (NaCl) (CAS N°:7647-14-5) and Sodium citrate tribasic dehydrate (CAS N°: 6132-04-3) were purchased at Sigma Aldrich. Cetyltrimethylammonium bromide (CTAB 98%) (CAS N°:57-09-0) from G BIOSCIENCES and Citric acid monohydrate (CAS N°: 5949-29-1) from Fluka. Ammonia 28% and Ethanol Absolute were purchased from VWR Chemicals, Whatman 1 filter paper from Cytiva (Ø 90 mm, Cat. 1; CAS N°: 1001-090). All the chemicals purchased were of analytical grade and were used without further purification. Milli-Q® water was used for all the experiments, treatment processes and storage (unless mentioned otherwise).

Synthesis of gold and silica nanoparticles (AuNPs and SNP) respectively:

These classical synthesis are described in the supporting information part 1, 2, Figure SI-1 and Figure SI-2.

Synthesis of isotrope gold/silica particles (ISO):

Isotrope gold/silica particles (called isotrope and ISO) are synthesized in 2 steps. First, a soft APTES functionalization of the particles surface in water is adapted from Bottero et al protocol [19], and secondly the AuNPs are attached on the functionalized particles. For APTES functionalization, the silica nanoparticles (SNP) stock suspension is prior redispersed by 10 min in ultrasonic bath (at 37 Hz, 60% power). We had previously checked that these conditions did not lead to particle degradation (see Figure SI-3). Then, in a Teflon flask, 0.5ml of the prepared SNP suspension is added to 50 ml of ethanol (7%v/v) /water mixture, vortex mix for 30 sec followed by the addition of 1 mL APTES (this excessive quantity of APTES is to ensure 15 APTES nm^{-2}) [19]. The suspension is let on a rotatory agitator for 18 hours at 50 rpm. Finally, excess APTES is removed through centrifugation/washing cycles, with centrifugation at ~11000 RCF (7000 RPM) for 15 minutes, two ethanol washing and the final one in water. The obtained (clean) SNP-NH_2 are redispersed in 10ml water and store in the fridge at 6°C for further usage. For AuNPs attachement, the SNP-NH_2 are first redispersed with ultrasonic bath, then 5 ml of the SNP-NH_2 suspension is kept under ultrasonic bath for 1-2 mn (at 37 Hz, 60% power) while 1 mL of the AuNPs suspension is added slowly. The resulting suspension is placed on a rotatory agitator at 50 rpm for 10 hours. Excessive AuNPs are removed by centrifuging at ~1400 RCF (2500 RPM) for 15 minutes and the pellet is resuspended in 5 mL of water. The particles ISO are characterized with SEM and EDX. Prior to their use, the suspension need to be under ultrasonic bath and vortex mixed.

Gold/Silica Janus nanoparticles with Chemical Synthesis:

The protocol used for producing the Janus particles is described in the Figure 1. First, wax colloidosomes stabilized by SNPs are produced (Pickering emulsion template), then functionalized with APTES. In a final stage, the wax is removed and AuNPs attached following the same protocol as for isotrope gold/silica particles.

 doi:10.20944/preprints202409.0820.v1

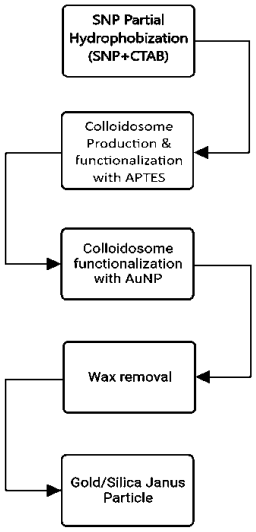

Figure 1. Summary flowcharts of chemical synthesis protocol for Gold/Silica Janus Particle via Pickering Emulsion Method.

Synthesis of colloidosomes:

The colloidosomes are synthesized following Avossa et al[20] procedure and previous literature on the subject [21–23]. In a 25 mL beaker, 20 ml of water and 2.5 ml of SNP solution (to attain the same surface as Avossa et al [20]) were mixed. The suspension is let under ultrasonic bath for 5 to 10 mn, (at 37 Hz, 60% power). Then, a chosen volume of Cetyltrimethylammonium bromide (CTAB) from a stock solution (C= 0.2 mM) is added to change the wetting properties of SNPs, and the mixture is stirred magnetically for 30 min at 50°C (1000 RPM). Several concentration of CTAB (from 0.005 mM to 0.08 mM) were tested to optimize the protocol, and the optimized final CTAB concentration is 0.04 mM. In a second step, the suspension is heated at 75°C and a pre-melted amount of wax corresponding to 0.08/10 in weight of water is added under Ultraturrax mixing. After 2 minutes at a power of 9500 rpm, the mixer is turned off and the emulsion quenched in 100 mL of cold water. Then, the suspension is filtered on Buchner with a Whatman filter (Cat. 1; CAS N°: 1001-090) and rinsed with ≈150 mL of water. Finally, the solid is recovered and left to dry at room temperature. The final product is characterized with SEM on roughly 60 colloidosomes measured.

Synthesis of Janus SNP-NH_2 particles:

We use the same soft protocol in water as for isotrope particles, derived from Bottero et al to graft (3-Aminopropyl) triethoxysilane (APTES) on the silica embedded in the wax. 0.5 g of colloidosomes is dispersed in a total volume of 50 mL of EtOH (7% v/v) /H_2O mixture in a Teflon flask followed by the addition of 0.2 ml APTES (in excess to be above 15 APTES per nm^2). The suspension is let on a rotatory agitator at 50 rpm for 18 hours. Then, the suspension is filtered on Buchner with a Whatman filter (Cat. 1; CAS N°: 1001-090) and washed with ethanol to remove the excess of APTS. To recover the functionalized Janus SNP-NH2 nanoparticles, the wax is removed with hexane. The powder is added to ≈40 mL of hexane in a polypropylene centrifuge tube (Vt=50mL), let in a ultrasonic bath (37 kHz) for 30 min and vortexed right after. The NPs are extracted and washed from two centrifugation (7000 RPM for 15 mn)/washing cycles. The 2 first cycles are done with hexane and the last one with ethanol. At the end, the suspension is centrifugated a last time and redispersed in water. This last step is repeated one time and ≈10 mL of water is added to concentrate the solution of Janus SNPs-NH_2. The particles were stored in the fridge and characterized by DLS, IR, and SEM.

Synthesis of Janus SNP-AuNPs particles (JP):

To partially functionalize silica nanoparticles with gold, the same protocol as for isotrope SNP particles have been used on the Janus SNP-NH_2 particles. 5mL of the SNPS-NH_2 suspension is placed in a Falcon tube under sonication while 1mL of the gold suspension is added slowly. The suspension

 doi:10.20944/preprints202409.0820.v1

is left for 1-2 minutes before adding another 1mL of AuNPs suspension to reach a total volume of 5 mL added in the end. Finally, the Falcon tube is left on the rotatory agitator at 50 rpm for 10h. To remove excess AuNPs, the suspension is centrifuged at 2500 rpm for 15 min. If the solution is clear, all the AuNPs have reacted. If it has a pink color, it means an excess of AuNPs. The supernatant is replaced with water and centrifuged again. This procedure is repeated three times before concentrating the Janus particles in 5mL of water. The Janus particles produced were then stored in the fridge before further characterization (SEM, EDX, UV, etc.).

Synthesis of Janus Gold/Silica nanoparticles with Physical Protocol (JP-PVD):

To produce Janus particles made of a thin gold layer covering partially the silica particles, a physical vapour deposition method was used. 200 µl of the silica particles suspension are first deposited by spincoating on a glass slide at 500 RPM for 10 sec, followed by 3400 RPM for 30 sec. The glass slide was prior cleaned under plasma treatment with oxygen (1 minute plasma under 50W power and 7.86 e^{-1} torr Pressure). The obtained SNP glass coated glass slide was let in into a Physical Vapour Deposition device at 10^{-6} mbar pressure and 100 – 140 A current running in the crucible to deposit 0.5 nm thick chromium layer at the rate of 0.5 angstrom/second, followed by 20 nm thick gold layer deposition from top at 1.6 to 1.9 angstrom/second deposition [24,25]. To recover the Janus particles, the glass slide was deposited into 10 ml water in a petri dish placed under ultrasonic bath for 30 min (37Hz, 100%).[26] The diluted suspension of Janus particles collected into a polypropylene centrifuge tube are centrifuged 15 min ~8064 RCF (6000 RPM). The pellet is redispersed in 1ml of Milli-Q®water and stored in the fridge. The particles are finally characterized by SEM.

Characterization techniques:

Scanning electron microscopy (SEM):

A ZEISS Ultra 55 equipped with a field emission gun (FEG), coupled with a Bruker EDX (Energy Dispersive X-ray Spectrometry) was utilized for SEM analysis of the particles. 1.5 kV and 10kV EHT (Electron High Tension) was maintained during characterizations. Either carbon tape or silicon wafer (surface cleaned via UV-ozone cleaner for 45 secs) [27] were used as sample substrate. 1 µL particle suspension (after 15 minutes ultrasonic bath) were dried on sample substrate during sample preparation for each SEM observations.

Dynamic light scattering (DLS), measurement:

A Zetasizer Nano Series Nano from Malvern Panalytical (Laser wavelength 633 nm) was utilized for the DLS measurements using the configuration of backscattered angle of 173° (NIBS default), 25° C temperature and equilibration time of 2 minutes. The measurements proceeded after a dilution step in Milli-Q®-water (refractive index (1.33) and viscosity (0.89 mPa.s). The particles concentration were adapted for each categories to have an optimized signal (mean count rates of scattered lights for optimal dilution was maintained from 160 to 480 kcps). The experiments were realized by preparing fresh samples before each DLS observation . To mitigate the risk of dust and contamination, new plastic container were used in each experiments and before using new containers, they were rinsed thrice (with milli-Q® water). This precautionary measure was followed to ensure the integrity of the experimental setup and minimized the impact of contaminants on DLS measurements [28,29]. First correlograms are registered with 3 repeated experiment measurements including 3 analysis for each. Then, size distribution have been extracted using the Methods of Cumulants for AuNPs and SNPs [30]. For the other particles a particular treatment has been used (see DLS paragraph).

For the case of measurements in presence of H_2O_2, particles were first submitted to ultrasonic bath for 5 mn and vortexed for 10 s, then added to Milli-Q® water/H_2O_2 mixture prior mixed with a glass tip for 10 secs (to avoid metal contamination to which H_2O_2 is very sensitive). The concentrations of H_2O_2 were 0% H_2O_2, 0.5% H_2O_2, 1% H_2O_2 and 5 % H_2O_2 for SNP; Iso, JP and JP-PVD.

Dynamic light scattering (DLS), data treatment:

Correlogram; autocorrelation function (C), is a function of lag-time (Δt) and can be described by Eq.1 where A is the scattering amplitude (normalized factor), B the instrumental factor, q the scattering vector (Eq. 2) and D the diffusion coefficient. The diffusion coefficient can be calculated

 doi:10.20944/preprints202409.0820.v1

from DLS correlogram fitting using Eq 1 plus 2 [31,32]. The scattering vector q for the set-up is 2.62 x 10^7 m^{-1} (calculated from Eq. 2 where n is refractive index (1.33), θ is detector angle detector (173°), and λ is wavelength (633 nm)). The theoretical values of diffusion coefficient for translational diffusion can be calculated from Stokes-Einstein equation (Eq. 3) [33], and linked to the particles diameter. where k_B is the Boltzmann constant (1.380649 × 10^{-23} $m^2kg/(K.s^2)$), T is Temperature (298 K), μ is the dispersant-viscosity (0.00089 kg/(m.s)) [34] and R the hydrodynamic radius of the particle (m).

$$C(\Delta t) = A\, e^{(-2Dq^2\Delta t)} + B \qquad \textit{(Eq 1)}$$

$$q = \frac{4\pi n}{\lambda}\left(\sin\frac{\theta}{2}\right) \qquad \textit{(Eq.2)}$$

$$D = \frac{k_B T}{6\pi\mu R} \qquad \textit{(Eq.3)}$$

The particles are also subject to rotational diffusion with a characteristic timescale $\tau_R^{-1} = k_BT/(8\pi\mu R^3)$.

Hence for anisotropic object, the decay of the correlation function contains the superposition of translational and rotational motion [35]. These 2 contributions could only be separated from depolarized dynamical scattering.

If fitting by one exponential decay is too poor, a double exponential decay is used. This happens for the Janus, ISO and JP-PVD particles as shown in results part.

Experiment: Particle Tracking Velocimetry (PTV):

PTV analysis were obtained in a channel included in a PDMS (Polydimethylsiloxane) microfluidic chip (~45 μm and 180 μm channel height and width, respectively) made by soft lithography protocol [36]. Prior to the measurements, particles suspension are filtered (pore size 0.65 μm) and diluted in Milli-Q® water (1:2 for SNP, 1:1 for ISO and JP) to eliminate any particle-aggregates that could have formed due to aging of samples. Particles/water/H_2O_2 suspensions are prepared just before the analysis by mixing 0, 17 and 22μL H_2O_2 with 100, 83 and 67 μL particle suspension to attain 0%, 5% and 10% (v/v) H_2O_2 respectively. The obtained suspensions are mixed manually for 10 seconds with micropipette prior to analysis. Then, samples are flowed in the chip by bringing pressure at 1mBar. The flow is stopped after 1 min to avoid convection driven motion in particle and measurements of particle-motion were done after 2 min stabilization time at ambient pressure. Conditions for imaging are 10 ms of camera exposure, frame rate at 10 FPS (frames per second) and record 200 images at 40x magnification. The intensity of the microscope-lamp has to be minimized as light induced decomposition of hydrogen peroxide and motion from thermal effects. The experimental protocol was validated on the pristine silica particles.

Data Treatment (PTV), Image processing (TrackMate):

The PTV study is in 2D and sticking of particle on the surface of glass slide is inevitable, therefore imaging in the region of interest (ROI) was chosen away from channel boundaries. After preliminary adjustments (image brightness, contrast) images were observed through TrackMate-ImageJ for tracking particle trajectories [37]. For this purpose pixel width, height and voxel depth was calibrated to unit value. Further, LoG detector, object diameter, quality threshold, tracker was set followed by the optimal criteria settings of the tracker type. In this PTV apparatus, simple LAP tracker was utilized to benefit in gap-closing between spots, linking-distance; beneficial for our 2D set-up with particles appearing-disappearing within close proximity. Lastly, information like particle-track, speed, travelled-distance, etc. (obtained as .csv output) were processed on Python platform PyCharm.

 doi:10.20944/preprints202409.0820.v1

As the frame rate (10 Frame per Second "FPS"), exposure time (10 ms) and pixels per µm (6.67) were known values, speed obtained from TrackMate (Track Mean Speed) was converted from 'pixels per frame' to 'µm/s' using Eq. 6 (a to c), followed by calculation of mean diffusion coefficient using Eq. 7 and the mean square displacement (MSD) [38,39], fromEq. 8, with n the number of dimensions (2), D the diffusion coefficient and T_d the Time interval per frame (0.09s). MSD is derivable from Velocity^2 x Time^2, comparing with Eq. 7 we get Eq (8) [40].

$$\text{Time per frame} = \frac{1}{\text{frame rate}} \quad \textit{(Eq.6 a)}$$

$$T_d = \text{Time per frame} - \text{Exposure time} \quad \textit{(Eq 6 b)}$$

$$v\left(\frac{\mu m}{s}\right) = Speed\left(\frac{px}{frame}\right) \times \frac{pixel_{size}}{T_d} \quad \textit{(Eq 6 c)}$$

$$D = \frac{v^2 T_d}{2n} \quad \textit{(Eq 7)}$$

$$MSD = 2nDT_d \quad \textit{(Eq. 8)}$$

Data Treatment (PTV), Data Processing (Python):

Particle trajectories (obtained from TrackMate-Spot Result) was repositioned to origin axis (zero, zero Cartesian coordinates) by fetching the respective x and y coordinates and combining it with its respective displacement-paths for analysis For example, Figure 2 shows native trajectories for observed SNP (in 0% [H_2O_2]).

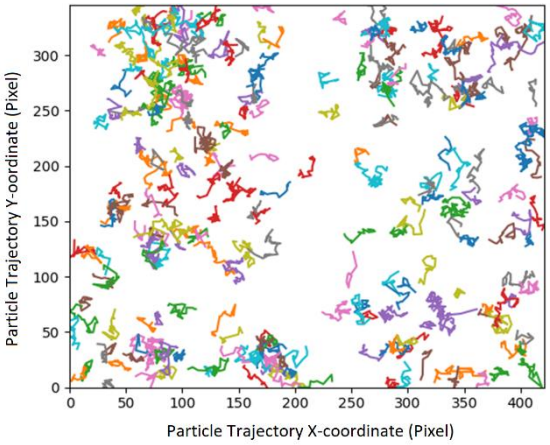

Figure 2. Trajectories of SNP in 0% H_2O_2 from Tracking as given by TrackMate.

Result and Discussion:

Particle preparation:

Silica particles half covered by gold (Janus particles) and isotropic particles (ISO fully covered by gold) were formulated to compare their properties. The particles are produced through attachment of gold nanoparticles (AuNPs) or from the deposition of a thin layer of gold on a silica particles. Four classes of particles were synthesized: pristine silica, isotropic AuNPs/Silica particles ("called ISO"), Janus AuNPs/Silica particles ("called JP") and Janus thin Au layer/Silica particles ("called JP-PVD") (see Figure 3 for the scheme of the different synthetic pathways). The silica particles were classically synthesized following the classical Stöber method [41,42] to produce 475±50 nm size particles (Figure SI-1 and Figure SI-2). The AuNPs of ~25 nm stabilized by citrate were synthesized using a reverse Turkevich protocol from Sivaraman et al [43] (Figure SI-4).

 doi:10.20944/preprints202409.0820.v1

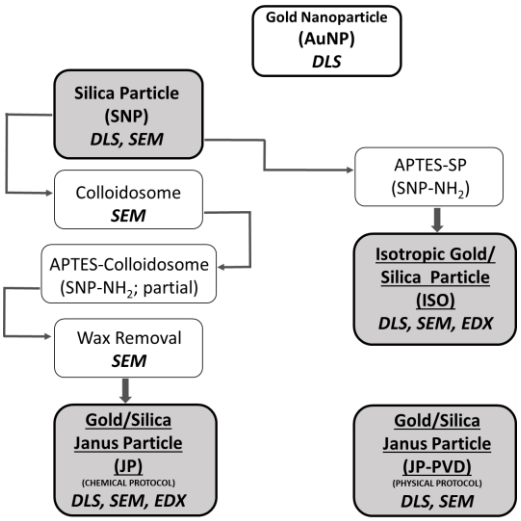

Figure 3. Flowcharts of strategy used for Janus Particle Synthesis via Pickering Emulsion Method and in bold, the characterisation methods.

The attachment of gold nanoparticles on the silica were obtained through the same chemical procedure for Janus and isotropic particles to ensure the similar linkage for both kind of particles. APTES is first grafted on silica surface in soft conditions (water and room temperature) following a protocol described by Cuoq et al [19] to produce silica particles functionalized with amine group. Then, preformed citrate gold nanoparticles are attached trough the amine function to the silica particles by mixing under sonication the amine grafted silica with the AuNPs water suspension. This procedure allows to obtain AuNPs-silica hybrid particles. When applied on isotropic amine grafted particles, isotropic AuNPs/Silica particles are obtained and characterized by SEM (Figure 5 a). For the Janus particles, a prior step is needed to ensure a partial grafting of silica particles by APTES. This can be achieved by the scalable wax pickering emulsion method developed for 100 to 500 nm silica particles by Ravaine et al [22,44] and initially proposed by Granick et al for larger silica particles [21]. It consists of attaching silica particles at the solidified wax/water interface of the so-called "colloidosome" to functionalize a part of the silica particle surface. Colloidosomes were obtained through the slight hydrophobization of the silica particles with CTAB, to produce an oil in water pickering emulsion above the melting point of the wax before a temperature quench in ice to solidify the wax. The optimal concentration of CTAB was identified by a combined zeta potential measure of silica coated with CTAB [20] (figure SI-5) and SEM analysis of the colloidosomes produced for 4 CTAB concentrations below the CTAB critical micellar concentration (cmc) (Figure SI-6, SI-7 and SI-8). 0.02 mM and 0.04 mM CTAB produced well defined colloidosomes for the chosen wax (Figure 4). The monolayer of partially embedded SNPs in 0.04 and 0.02 mM CTAB (observed at higher magnification in (Figure 4b and d), respectively) confirms SNP wettability altered via aliphatic chains of CTAB. The size of the colloidosome in function of the CTAB concentration is summarized in Figure SI-9 and Table SI-1).

 doi:10.20944/preprints202409.0820.v1

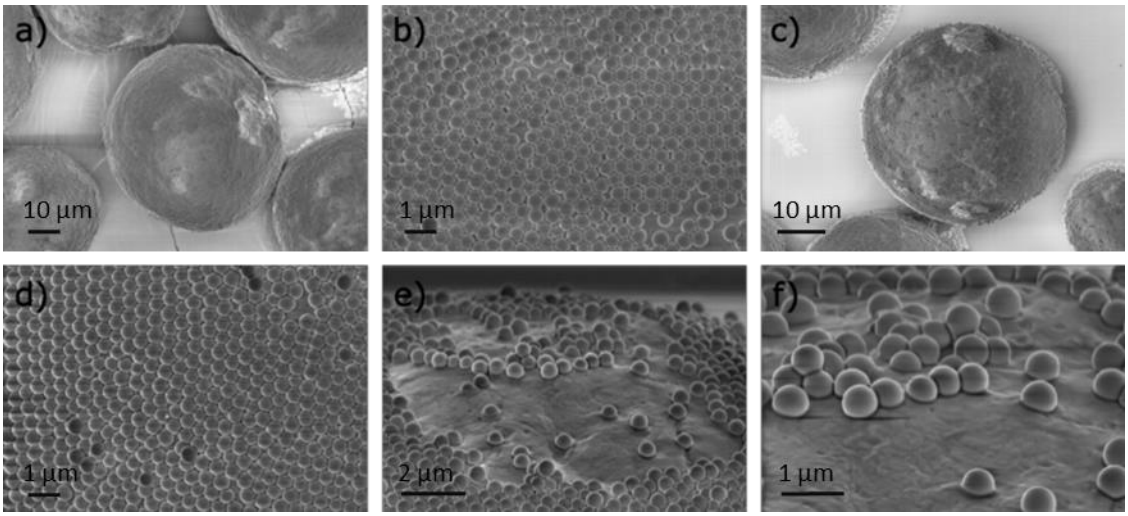

Figure 4. SEM images of the colloidosomes: a) b) colloidosome and its surface synthesized at 0.04mM. c), d) colloidosome and its surface synthesized at 0.02mM and e), f) a closer look on the embedment of silica particles for 0.02mM CTAB.

The colloidosomes serve as a plateform for partial grafting of the silica particles. The surface of silica not embedded in the solidified wax is grafted with APTES in soft conditions similar to the conditions used for isotropic particles. The Janus SNP-NH_2 particles were isolated by dissolving wax in hexane (Figure SI-10). Finally, the Janus SNP-NH_2 particles were functionalized by AuNPs through the addition of preformed AuNPs to the Janus SNP-NH_2 water dispersion in an ultrasonic bath. For Janus synthesis, the experimental parameters (CTAB concentration, silica concentration, ultraturax energy, APTES concentration, AuNPs concentration, ultrasonic mediation, etc ..) were optimized to ensure the reproducibility of the Janus particles production from one batch to another. The Figure 5 shows the SEM characterizations of isotrope and Janus particles made of silica particles with grafted AuNPs. The gold and Si identification was verified by EDX for isotrope and Janus particles (Figure SI-11 and SI-12 respectively), however quantification was not possible because of the Si wafer used for the analysis.

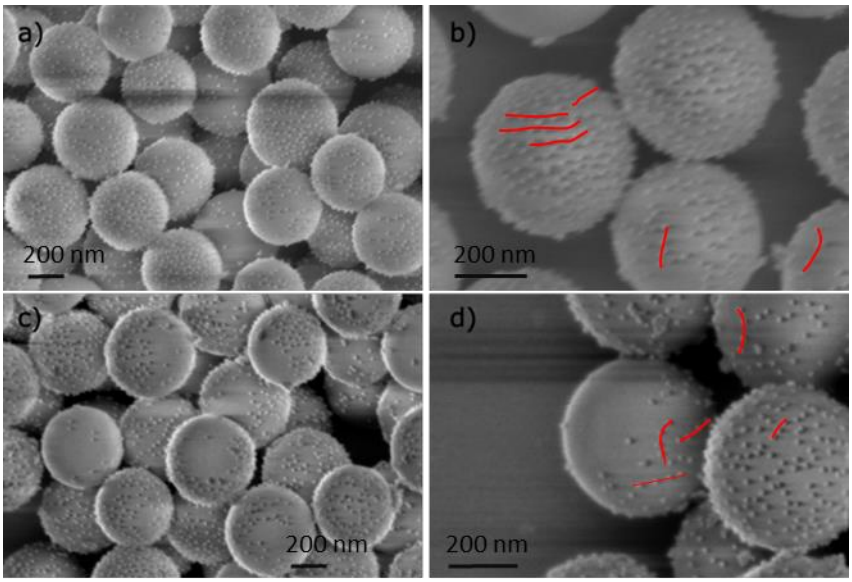

Figure 5. SEM images of a),b) isotrope silica nanoparticles functionalized with AuNPs (ISO) and c),d) Janus AuNPs/silica nanoparticles synthesized from colloidosomes strategy (JP). The red lines show the particle alignments.

 doi:10.20944/preprints202409.0820.v1

The silica coverage rate by AuNPs and the average distance between grafted AuNPS can be extracted from the SEM images. Distance between particles can be directly measured on the SEM images or calculated in average from the number of AuNPs per SNP. The Table 1 summarizes the obtained values.

Table 1. Organisation of the AuNPs functionalized SNP. AuNPs/SiO_2 is the number of AuNPs per silica particles counted from visible part in SEM images and d_{cc} the average distance between the centers of 2 AuNPs on silica particles measured when particles are aligned or in average from the counted AuNPs on SiO_2 particles..

Particles	AuNP/SiO2 NP	Au-Au center to center distance (d_{cc} in nm) (-)
SiO2_AuNPS_iso (iso)	(*) 220 - 280	~ 35 to 40 nm
SiO2_AuNPS_Janus (JP_AuNP)	(+) 110 - 150	~ 35 to 40 nm

(-).The batch used for analysis was prepared with AuNPs size of ~ 20 nm.

The number of gold Nanoparticles per SNP, for isotropic and Janus differs by approximately a factor 2 (see Table 2). The face to face distance between AuNPs is slightly inferior to the size of AuNPs diameter for both kind of particles ensuring that the produced particles are similar and only differ by the presence of an area of depleted of AuNPs for JP. The minimal distance between the AuNPs results from the equilibrium between VdW interaction and electrostatic repulsion between AuNPs (for 25 nm AuNPs size, the equivalence of the VdW potential with thermal energy is at 20 nm and for 20 nm AuNPs size, it is 15 nm) [45,46]. However, this minimal distance does not result in an 2D organized paving of the space, but rather as lines of AuNPs, that may reveal a subsequent order in the SNP or in the grafting process. Multiple SEM observations of JP highlighting distinctive asymmetric assembly of gold nanoparticles with minimal aggregates confirms that the protocol is successfully robust and reproducible with an efficiency for bulk quantity of around 100 mg Janus Particles with little variation from one particle to another. Recently, Trihan et al [47] have shown that hetero-aggregation between amine functionalized silica particles and citrate stabilized gold nanoparticles is efficient to optimize the total gold density and homogeneity, emphazing the particle size ratio silica/gold to minimize the curvature effect. They obtained an isotropic surface coverage density of 15% with smaller AuNPs size (8 nm) on SiO_2 particles of 600 nm. In our case, we attain a surface coverage density between 7 and 10% for ISO and Janus particles, a number in the same range of order of the one obtained by Perro's et al [22] from bulk synthesis with colloidosomes. From their TEM images, 72 AuNPs (of 15 nm) can be counted with a ~ 15 nm face to face distance on Silica particles of 250 nm. With a different approach based on liquid/liquid interface in a microfluidic device, Abou-Hassan et al synthesized Au-SiO2 Janus particles with a surface coverage density of ~ 10% [48].

In the literature, Janus particles have been highly reproduced from the Perro's protocol based on solidified emulsion pathway, with however few characterisation on the Janus particles. Our originality here is to produce a family of particles with 2 different coverage rates (half and total surface) produced by similar grafting process.

Another kind of Janus particles were produced by Physical Vapour Deposition methods (PVD) of gold on spin-coated SNP on glass. The gold layer is deposited on a prelayer of chromium to ensure a good adhesion. A layer of 20 nm thickness gold was deposited, a value chosen to be close to the size of the gold NPs in the isotropic and Janus AuNP/SNP. Lastly, ultrasonication of the glass slide (submerged in Milli-Q® water) ensured maximum extraction of physically produced gold/silica janus particles (PVD). The PVD Janus particles were caracterized by SEM (Figure 6).

 doi:10.20944/preprints202409.0820.v1

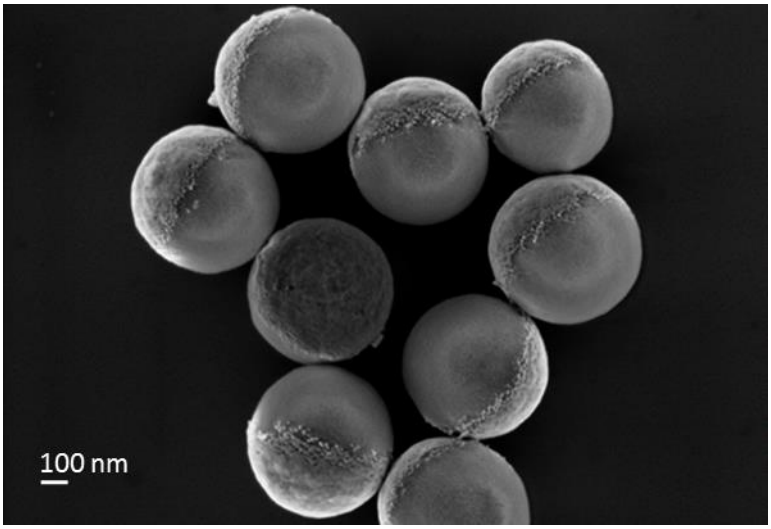

Figure 6. SEM images of JP-PVD Janus gold functionalized SNP.

Because of the sub-micron size of the particles, Focused Ion Beam (FIB) can not be used for the characterisation of the gold layer contrary to Rashidi studies on gold/polystyrene Janus particle of 5 µm diameter.[27] Therefore, rough estimation of deposited gold layer was achieved by calculating the thickness gold layer from SEM observation of 17 PVD particles. At the resolution of ~ 5.56 nm/pixels, the value for gold layer in central position is ~20±2 nm, and ~18±2 nm around the edges, which is due to the curvature of spherical silica particles. These values are in coherence with the targeted deposited value chosen for the physical vapour deposition.

Summary of the different class of synthesized particles:

A family of 4 different particles have been synthesized. The Table 2 lists the particles and their characteristic features (Janus or not) and briefly highlights the methods followed and the learning outcomes as important factors for the reproducibility. The Janus-PVD (JP-PVD) particles are heavier by nearly a factor two in comparison to Janus-AuNPs (JP).

Table 2. Summary of key factors in the methods followed for synthesising different particles.

Type of particle, Averaged particle size and weight	***Method***	***Important Factors for reproducibility. Reproducibility achieved***	***Maximal amount that can be prepared Time for preparation***
AuNP 25nm, 1.6 10^{-16} g	Reverse Turkevich	Gold/citrate ratio, temperature, citrate concentration. +- 4nm from batch to batch	10 ml or 50 ml of AuNPs suspension at 0.25 mM in Au per batch Time for preparation ~ 1h (after 1 day of rest)
SNP 475nm, 1.2 10^{-13} g	Stöber	TEOS/EtOH/H2O ratios and Precursors Mixing Rate.	30 ml of silica NPs (475 nm) suspension at 30 mg/ml in SiO_2 ie 2.4 10^{11} part/ml. **(~ 900 mg of SiO2 NPs per batch**)

 doi:10.20944/preprints202409.0820.v1

			Time for preparation ~4 H
Iso **480nm 1.6 10^{-13} g**	Surface functionalization	1. APTES Catalysis and AuNPs concentration and APTES 2. Interaction time (with APTES and with AuNPs) 3. Stability of the SNPs Number of grafted particles: 220-280	2 steps: functionalization by NH2 and then AuNPs grafting. 5 ml of Iso at 1.22 10^{10} part/ml ~ **~10 mg of iso from 7.5 mg of SiO_2.NPs** Time for preparation: 1,5 day
JP **478nm 1.5 10^{-13} g**	Pickering Emulsion And surface functionalization	1. Molar ratio of SNP:CTAB (for Colloidosome preparation), mass ratio of SNP:Water (for SNP functionalization with APTES) and mass proportion of SNP:Wax:Water (for APTES-SNP functionalization with AuNP) 2. Solvent for APTES 3. Emulsification energy (for Pickering Emulsion) 4. Quenching of emulsion 5. Solvent for Wax removal Number of grafted particles: 110-150	Need first the preparation of colloïdosomes.: ~2 to 3 g of colloidosomes per batch. Time for preparation: 2 days 0.5 g of colloidosomes used to obtain at the end 5 ml of Janus-AuNPs at ~ 1.6 10^{13} part/ml (~ **20 mg of JP from 0.5 g of colloidosomes**) Time of preparation: Janus-AuNPs: 1,5 day
JP_PVD **485nm 2.7 10^{-13} g**	Physical Vapor Deposition	1. Monolayer assembly of SNP on substrate 2. Intermediate adhesion layer between Gold and SNP Thickness of gold layer : 20 nm +- 1 nm	~1.7 10^{10} particles/batch (from a 37.5 cm^2 glass coating) Ie 1 ml of suspension at 1.7 10^{10} particles/ml (**~4.4 mg per batch**) Time of preparation: 2 H

 doi:10.20944/preprints202409.0820.v1

Mobility in bulk solution:

The mobility of the four type of particles was studied by dynamic light scattering in the presence or the absence of H_2O_2. DLS has indeed the capability to characterize micro and nano motor motions. The correlation curves were fitted in most cases by one exponential, with a correlation time in the 7. 10^{-4} s range. However, in some cases, a second exponential had to be added to adjust the signal, with a correlation time in the 3. 10^{-1} s range (see Table SI 2) for the values and Figure 7 for a typical example of one and double exponential fitting).

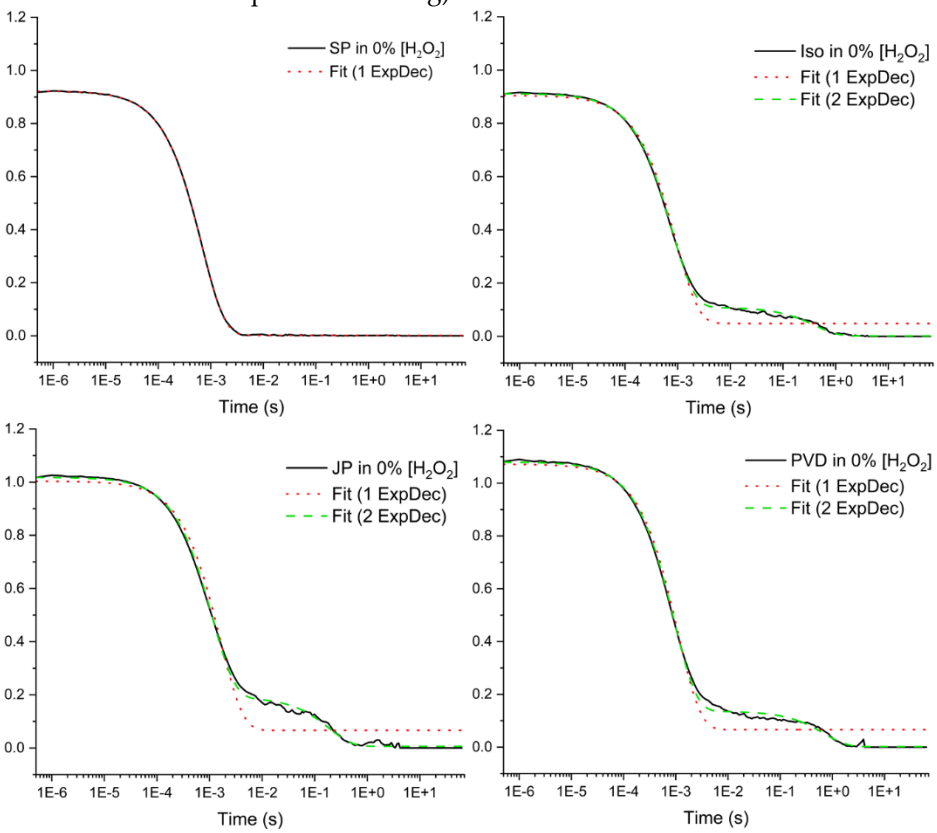

Figure 7. Curve fitting of respective samples at 0% H_2O_2. Black solid lines represents mean correlograms from DLS experiment. Red dotted lines represents curve-fit with single exponential decay function and green dashed-lines represents curve-fit with double exponential decay function. Curves fitting better with double exponential decay function.

This two exponential behaviour appears in the literature for particles having a significant degree of anisotropy. One DLS signal is coming from the translation motions and one from the rotational motion. For the size of particles considered and the order of magnitude of the relaxation times that can be deduced from Eq 3 and 1, the fast signal can be assigned to translational motions and the slow one to rotational motions (when it is observed). However, the exact exploitation of the rotational component requires both polarized and depolarized DLS measurement that were not conducted here [35,49,50]. Therefore, only translational diffusion constants are presented in Table 3.

In the absence of H_2O_2, the diffusion coefficient can give access to the hydrodynamic radius through Stokes Einstein relationship. The radii measured are very near from the geometric ones expected for JP particles (see Table SI 3) which reached 700 nm! One explanation could be that the Janus particle present a unique heterogenitity of interfacial energy that is, in simulations, expected to impact their diffusion behaviour [51]. We may connect this specific interfacial energy to the colloidosomes process that might leave residual wax on the surface. Another explanation could be that the pronounced asymmetry of these particles could reinforce the rotational DLS signal for these samples, leading to an apparent enlargement of the translational signal.

In the presence of H_2O_2, we observed a significative evolution of the diffusion coefficient for ISO and JP. Their maximum increase in diffusion is of about 30% and is achieved at 1% in H_2O_2.These

 doi:10.20944/preprints202409.0820.v1

values are in agreement with other, Janus systems composed of gold [49] and ten times lower than the one obtained on Pt. No signitificative variation was observe for SNP, which was expected and JP-PVD, which was more surprising.

Table 3. Translational diffusion coefficient obtained from the DLS correlogram analysis for different H_2O_2 concentration. Higher concentrations could not be measured owing to the formation of bubbles.

% (v/v)	Diffusion Coefficient (⌾m²/s) ± Std. Dev (%)			
[H_2O_2]	**SNP**	**Iso**	**JP**	**JP-PVD**
0	1.05 ± 2.2	1.03 ± 5.4	0.70 ± 8.5	0.86 ± 6.2
0.5	1.07 ± 1.3	1.25 ± 6.5	0.80 ± 7.4	0.86 ± 6.8
1	1.05 ± 1.4	1.32 ± 12.5	0.88 ± 15.2	0.90 ± 5.1
3	1.05 ± 2.0	1.22 ± 1.0	0.89 ± 9.4	0.86 ± 3.0
5	1.06 ± 2.4	1.23 ± 2.1	0.90 ± 5.0	0.85 ± 4.2

Mobility in microchannels:

A particle tracking velocimetry experiment (PTV) was developed in parallel to give access to a second method of diffusion measurement. These PTV measurements were conducted in microchannels (see Materials and Methods) in order to supress any possible collective effects and Marangoni flows due to evaporation [52]. We must first notice that the uncertainties associated to these measurements are much higher than in DLS. This is due to known problems in sampling in PTV measurements [53] that might covers only a part of the tracking times available on DLS which is the case in our study. The obtained values are summarized in Table 4.

If we consider now only the averaged values of diffusion coefficient in the absence of H_2O_2, the values for SNP, ISO and JP are quite similar in DLS and PTV. However, the one for JP-PVD are too far from the expected range to have a physical meaning. Due to the acquisition time used for the JP-PTV (~100ms), we may observe here gravitational effects due to the large weight of the particles (see Table 2) [54].

In the presence of H_2O_2, the increase on ISO and JP diffusion (20-30%) is also compatible with the one measured by DLS in the 1-5% H_2O_2 range. However, JP appear much more efficient at very high H_2O_2 concentrations, reaching 110% increase in diffusion.

Table 4. Diffusion coefficient obtained from PTV analysis for different H_2O_2 concentration. .

% (v/v)	Diffusion Coefficient (⌾m²/s) ± Std. Dev			
[H_2O_2]	**SNP**	**Iso**	**JP**	**JP-PVD**
0	0.96 ± 0.45	0.68 ± 0.41	1.04 ± 0.79	3.10 ± 1.87
5	0.91 ± 0.40	0.77 ± 0.94	1.40 ± 0.87	3.38 ± 1.25
10	0.93 ± 0.48	0.81 ± 0.69	2.33 ± 1.27	2.32 ± 2.94

Comparison:

Our approach, based on a common synthetic platform, first revealed bias in the values measured in both methods used in particle motion qualification for Janus particles, DLS and PTV. However for both techniques, variation in diffusion coefficient is visible for gold functionalized SNP particles in the presence of H_2O_2, ensuring an effect of the reactivity between gold and H_2O_2.The chosen approach

 doi:10.20944/preprints202409.0820.v1

also demonstrated that the explicit preparation of Janus structure is not mandatory to obtain a motion at intermediate fuel concentration. In Table 4, it is indeed shown that Janus particle are only marginal faster that the so-called ISO ones. However, if isotropic particles can achieve motion in chemical gradients, asymmetry is theoretically mandatory if the concentration in fuel is homogeneous [16]. We can therefore consider three different possible hypothesis to explain the motions:

1) The catalytic activity create local gradient due to insufficient mixing during the measurement. However, it can not be the case in microfluidic experiments as particles explore all the space of the channels.

2) The catalytic activity is sufficiently low to occur at the same time only on a limited number of spots on the particle. The low number of spots distributed randomly will thus create an asymmetry. If it may not be sufficient for the production of a local chemical gradient, this may lead to asymmetric local heating, and thus to thermophoresis. This may explain why ISO and JP have similar efficiency at intermediate concentration in fuel (< 5%), but not at high concentration (10%) were the reactive sites will be more synchrone.

3) The AuNPs are not distributed evenly enough on the silica surface to ensure a real isotropy. This hypothesis was indeed introduced to explain the chemotaxis of PLGA gold particles [14]. The main argument for this is the observation of a rotational component in ISO DLS signal that is the signature of anisotropy. The defects in the organization of the AuNPs on ISO particle are sufficient to provide them with their motion capabilities.

Our result do not allow to distinguish between the two latter explanation and may be a combination of the two phenomena.

Conclusions

A family of different silica particles functionalized by gold were synthesized to compare their mobility in the presence of H_2O_2. The design of the particles were chosen 1) to ensure similar grafting of gold nanoparticles for isotropic and Janus configuration and 2) to produce Janus particles with 2 different gold functionalization (gold nanoparticles and gold layer whose thickness is equivalent to the AuNPs diameter ~20 nm). The mobility were compared through DLS (3D in batch) and PTV analysis (in a microfluidic channel to avoid collective effect). Whatever the functionalization, the particles are mobile in the presence of H_2O_2. If analysis revealed bias in the values measured in both methods (DLS and PTV), a general trend can be observed showing that for intermediate fuel concentration, Janus structure is not mandatory to obtain a motion. The mechanism at work needs further investigation but open promising possibility for the design of self-propelled particles.

Author Contributions: Conceptualization, project administration, writing_original draft preparation, methodologies, analysis, funding acquisition and supervision: JR, FM, FT; Synthesis of Janus particles, writing: AA, development of python codes forData Treatment (PTV, TrackMate) : ZAA, DLS analysis, methodologies, PG; Synthesis, characterizations, image processing, mobility measurements (DLS, PTV), data analysis, figure preparation and writing: VN. All the authors have read and agreed for the published version of the manuscript.

Acknowledgment: We thank Miguel Comesaña-Hermo from ITODYS, University Paris Saclay for his help to the Stöber synthesis and Vincent Mertens for his introduction and teaching of the SEM experiments .We thank the nuclear decommissioning program of CEA for its financial support.

References

1. Elgeti, J.; Winkler, R.G.; Gompper, G. Physics of Microswimmers—Single Particle Motion and Collective Behavior: A Review. *Rep. Prog. Phys.* **2015**, *78*, 056601, doi:10.1088/0034-4885/78/5/056601.
2. Pourrahimi, A.M.; Pumera, M. Multifunctional and Self-Propelled Spherical Janus Nano/Micromotors: Recent Advances. *Nanoscale* **2018**, *10*, 16398–16415, doi:10.1039/C8NR05196H.
3. Lee, E.; Huang, D.; Luo, T. Ballistic Supercavitating Nanoparticles Driven by Single Gaussian Beam Optical Pushing and Pulling Forces. *Nat. Commun.* **2020**, *11*, 2404, doi:10.1038/s41467-020-16267-9.

4. Yariv, E. Self-Diffusiophoresis of Slender Catalytic Colloids. *Langmuir* **2020**, *36*, 6903–6915, doi:10.1021/acs.langmuir.9b02393.
5. Kuron, M.; Kreissl, P.; Holm, C. Toward Understanding of Self-Electrophoretic Propulsion under Realistic Conditions: From Bulk Reactions to Confinement Effects. *Acc. Chem. Res.* **2018**, *51*, 2998–3005, doi:10.1021/acs.accounts.8b00285.
6. Wang, W.; Mallouk, T.E. A Practical Guide to Analyzing and Reporting the Movement of Nanoscale Swimmers. *ACS Nano* **2021**, *15*, 15446–15460, doi:10.1021/acsnano.1c07503.
7. Popescu, M.N.; Uspal, W.E.; Bechinger, C.; Fischer, P. Chemotaxis of Active Janus Nanoparticles. *Nano Lett.* **2018**, *18*, 5345–5349, doi:10.1021/acs.nanolett.8b02572.
8. Joseph, A.; Contini, C.; Cecchin, D.; Nyberg, S.; Ruiz-Perez, L.; Gaitzsch, J.; Fullstone, G.; Tian, X.; Azizi, J.; Preston, J.; et al. Chemotactic Synthetic Vesicles: Design and Applications in Blood-Brain Barrier Crossing. *Sci. Adv.* **2017**, *3*, e1700362, doi:10.1126/sciadv.1700362.
9. Baraban, L.; Harazim, S.M.; Sanchez, S.; Schmidt, O.G. Chemotactic Behavior of Catalytic Motors in Microfluidic Channels. *Angew. Chem. Int. Ed.* **2013**, *52*, 5552–5556, doi:10.1002/anie.201301460.
10. Hong, Y.; Blackman, N.M.K.; Kopp, N.D.; Sen, A.; Velegol, D. Chemotaxis of Nonbiological Colloidal Rods. *Phys. Rev. Lett.* **2007**, *99*, 178103, doi:10.1103/PhysRevLett.99.178103.
11. Perro, A.; Reculusa, S.; Ravaine, S.; Bourgeat-Lami, E.; Duguet, E. Design and Synthesis of Janus Micro- and Nanoparticles. *J. Mater. Chem.* **2005**, *15*, 3745–3760, doi:10.1039/B505099E.
12. Gao, C.; Feng, Y.; Wilson, D.A.; Tu, Y.; Peng, F. Micro-Nano Motors with Taxis Behavior: Principles, Designs, and Biomedical Applications. *Small* **2022**, *18*, 2106263, doi:10.1002/smll.202106263.
13. Mandal, N.S.; Sen, A.; Astumian, R.D. Kinetic Asymmetry versus Dissipation in the Evolution of Chemical Systems as Exemplified by Single Enzyme Chemotaxis. *J. Am. Chem. Soc.* **2023**, *145*, 5730–5738, doi:10.1021/jacs.2c11945.
14. Wang, J.; Toebes, B.J.; Plachokova, A.S.; Liu, Q.; Deng, D.; Jansen, J.A.; Yang, F.; Wilson, D.A. Self-Propelled PLGA Micromotor with Chemotactic Response to Inflammation. *Adv. Healthc. Mater.* **2020**, *9*, 1901710, doi:10.1002/adhm.201901710.
15. Jiang, H.; He, X.; Ma, Y.; Fu, B.; Xu, X.; Subramanian, B.; Hu, C. Isotropic Hedgehog-Shaped-TiO $_2$ /Functional-Multiwall-Carbon-Nanotube Micromotors with Phototactic Motility in Fuel-Free Environments. *ACS Appl. Mater. Interfaces* **2021**, *13*, 5406–5417, doi:10.1021/acsami.0c19606.
16. Deprez, L.; De Buyl, P. Passive and Active Colloidal Chemotaxis in a Microfluidic Channel: Mesoscopic and Stochastic Models. *Soft Matter* **2017**, *13*, 3532–3543, doi:10.1039/C7SM00123A.
17. Lyu, X.; Liu, X.; Zhou, C.; Duan, S.; Xu, P.; Dai, J.; Chen, X.; Peng, Y.; Cui, D.; Tang, J.; et al. Active, Yet Little Mobility: Asymmetric Decomposition of H2O2 Is Not Sufficient in Propelling Catalytic Micromotors. *J. Am. Chem. Soc.* **2021**, *143*, 12154–12164, doi:10.1021/jacs.1c04501.
18. Bianchi, G.; Mazza, F.; Mussini, T. Catalytic Decomposition of Acid Hydrogen Peroxide Solutions on Platinum, Iridium, Palladium and Gold Surfaces. *Electrochimica Acta* **1962**, *7*, 457–473, doi:10.1016/0013-4686(62)80034-6.
19. Cuoq, F.; Masion, A.; Labille, J.; Rose, J.; Ziarelli, F.; Prelot, B.; Bottero, J.-Y. Preparation of Amino-Functionalized Silica in Aqueous Conditions. *Appl. Surf. Sci.* **2013**, *266*, 155–160, doi:10.1016/j.apsusc.2012.11.120.
20. Avossa, J.; Esteves, A.C.C. Influence of Experimental Parameters on the Formation and Stability of Silica-Wax Colloidosomes. *J. Colloid Interface Sci.* **2020**, *561*, 244–256, doi:10.1016/j.jcis.2019.11.011.
21. Hong, L.; Jiang, S.; Granick, S. Simple Method to Produce Janus Colloidal Particles in Large Quantity. *Langmuir* **2006**, *22*, 9495–9499, doi:10.1021/la062716z.
22. Perro, A.; Meunier, F.; Schmitt, V.; Ravaine, S. Production of Large Quantities of "Janus" Nanoparticles Using Wax-in-Water Emulsions. *Colloids Surf. Physicochem. Eng. Asp.* **2009**, *332*, 57–62, doi:10.1016/j.colsurfa.2008.08.027.
23. Archer, R.J.; Parnell, A.J.; Campbell, A.I.; Howse, J.R.; Ebbens, S.J. A Pickering Emulsion Route to Swimming Active Janus Colloids. *Adv. Sci.* **2018**, *5*, 1700528, doi:10.1002/advs.201700528.
24. George, M.A.; Glaunsinger, W.S.; Thundat, T.; Lindsay, S.M. Electrical, Spectroscopic, and Morphological Investigation of Chromium Diffusion through Gold Films. *Thin Solid Films* **1990**, *189*, 59–72, doi:10.1016/0040-6090(90)90027-B.
25. Moody, N.R.; Adams, D.P.; Medlin, D.; Headley, T.; Yang, N.; Volinsky, A. Effects of Diffusion on Interfacial Fracture of Gold-Chromium Hybrid Microcircuit Films. *Int. J. Fract.* **2003**, *120*, 407–419, doi:10.1023/A:1024979829573.
26. Vikash; Kumar, V. Ultrasonic-Assisted de-Agglomeration and Power Draw Characterization of Silica Nanoparticles. *Ultrason. Sonochem.* **2020**, *65*, 105061, doi:10.1016/j.ultsonch.2020.105061.
27. Vig, J.; LeBus, J. UV/Ozone Cleaning of Surfaces. *IEEE Trans. Parts Hybrids Packag.* **1976**, *12*, 365–370, doi:10.1109/TPHP.1976.1135156.

28. Yu, Z.; Reid, J.C.; Yang, Y.-P. Utilizing Dynamic Light Scattering as a Process Analytical Technology for Protein Folding and Aggregation Monitoring in Vaccine Manufacturing. *J. Pharm. Sci.* **2013**, *102*, 4284–4290, doi:10.1002/jps.23746.
29. Farrell, E. Guide for DLS Sample Preparation.
30. Koppel, D.E. Analysis of Macromolecular Polydispersity in Intensity Correlation Spectroscopy: The Method of Cumulants. *J. Chem. Phys.* **1972**, *57*, 4814–4820, doi:10.1063/1.1678153.
31. Misono, T. Dynamic Light Scattering (DLS). In *Measurement Techniques and Practices of Colloid and Interface Phenomena*; Abe, M., Ed.; Springer: Singapore, 2019; pp. 65–69 ISBN 9789811359316.
32. Leong, S.S.; Ng, W.M.; Lim, J.; Yeap, S.P. Dynamic Light Scattering: Effective Sizing Technique for Characterization of Magnetic Nanoparticles. In *Handbook of Materials Characterization*; Sharma, S.K., Ed.; Springer International Publishing: Cham, 2018; pp. 77–111 ISBN 978-3-319-92955-2.
33. Kholodenko, A.L.; Douglas, J.F. Generalized Stokes-Einstein Equation for Spherical Particle Suspensions. *Phys. Rev. E* **1995**, *51*, 1081–1090, doi:10.1103/PhysRevE.51.1081.
34. Huang, X.; Sheng, L.; Lu, Y.; Li, S. Atomization Characteristics of Hydrogen Peroxide Solutions in Electrostatic Field. *Micromachines* **2022**, *13*, 771, doi:10.3390/mi13050771.
35. McGlasson, A.; Bradley, L.C. Investigating Time-Dependent Active Motion of Janus Micromotors Using Dynamic Light Scattering. *Small* **2021**, *17*, 2104926, doi:10.1002/smll.202104926.
36. Xia, Y.; Whitesides, G.M. Soft Lithography. *Angew. Chem. Int. Ed.* **1998**, *37*, 550–575, doi:10.1002/(SICI)1521-3773(19980316)37:5<550::AID-ANIE550>3.0.CO;2-G.
37. Tinevez, J.-Y.; Perry, N.; Schindelin, J.; Hoopes, G.M.; Reynolds, G.D.; Laplantine, E.; Bednarek, S.Y.; Shorte, S.L.; Eliceiri, K.W. TrackMate: An Open and Extensible Platform for Single-Particle Tracking. *Methods* **2017**, *115*, 80–90, doi:10.1016/j.ymeth.2016.09.016.
38. Michalet, X. Erratum: Mean Square Displacement Analysis of Single-Particle Trajectories with Localization Error: Brownian Motion in an Isotropic Medium [Phys. Rev. E **82** , 041914 (2010)]. *Phys. Rev. E* **2011**, *83*, 059904, doi:10.1103/PhysRevE.83.059904.
39. Nandi, A.; Heinrich, D.; Lindner, B. Distributions of Diffusion Measures from a Local Mean-Square Displacement Analysis. *Phys. Rev. E* **2012**, *86*, 021926, doi:10.1103/PhysRevE.86.021926.
40. Medved, A.; Davis, R.; Vasquez, P.A. Understanding Fluid Dynamics from Langevin and Fokker–Planck Equations. *Fluids* **2020**, *5*, 40, doi:10.3390/fluids5010040.
41. Stöber, W.; Fink, A.; Bohn, E. Controlled Growth of Monodisperse Silica Spheres in the Micron Size Range. *J. Colloid Interface Sci.* **1968**, *26*, 62–69, doi:10.1016/0021-9797(68)90272-5.
42. Muñoz, M.I. CRISTALES FOTÓNICOS BASADOS EN ÓPALOS. phD, Universidad Autónoma de Madrid, 2003.
43. Sivaraman, S.K.; Kumar, S.; Santhanam, V. Monodisperse Sub-10 Nm Gold Nanoparticles by Reversing the Order of Addition in Turkevich Method–the Role of Chloroauric Acid. *J. Colloid Interface Sci.* **2011**, *361*, 543–547, doi:10.1016/j.jcis.2011.06.015.
44. Perro, A.; Meunier, F.; Schmitt, V.; Ravaine, S. Production of Large Quantities of "Janus" Nanoparticles Using Wax-in-Water Emulsions. *Colloids Surf. Physicochem. Eng. Asp.* **2009**, *332*, 57–62, doi:10.1016/j.colsurfa.2008.08.027.
45. Ohara, P.C.; Leff, D.V.; Heath, J.R.; Gelbart, W.M. Crystallization of Opals from Polydisperse Nanoparticles. *Phys. Rev. Lett.* **1995**, *75*, 3466–3469, doi:10.1103/PhysRevLett.75.3466.
46. Derjaguin, B.V.; Rabinovich, Y.I.; Churaev, N.V. Direct Measurement of Molecular Forces. *Nature* **1978**, *272*, 313–318, doi:10.1038/272313a0.
47. Trihan, R.; Bogucki, O.; Kozlowska, A.; Ihle, M.; Ziesche, S.; Fetliński, B.; Janaszek, B.; Kieliszczyk, M.; Kaczkan, M.; Rossignol, F.; et al. Hybrid Gold-Silica Nanoparticles for Plasmonic Applications: A Comparison Study of Synthesis Methods for Increasing Gold Coverage. *Heliyon* **2023**, *9*, e15977, doi:10.1016/j.heliyon.2023.e15977.
48. Hassan, N.; Stocco, A.; Abou-Hassan, A. Droplet Liquid/Liquid Interfaces Generated in a Microfluidic Device for Assembling Janus Inorganic Nanohybrids. *J. Phys. Chem. C* **2015**, *119*, 10758–10765, doi:10.1021/acs.jpcc.5b02527.
49. Lee, T.-C.; Alarcón-Correa, M.; Miksch, C.; Hahn, K.; Gibbs, J.G.; Fischer, P. Self-Propelling Nanomotors in the Presence of Strong Brownian Forces. *Nano Lett.* **2014**, *14*, 2407–2412, doi:10.1021/nl500068n.
50. Feller, D.; Otten, M.; Hildebrandt, M.; Krüsmann, M.; Bryant, G.; Karg, M. Translational and Rotational Diffusion Coefficients of Gold Nanorods Functionalized with a High Molecular Weight, Thermoresponsive Ligand: A Depolarized Dynamic Light Scattering Study. *Soft Matter* **2021**, *17*, 4019–4026, doi:10.1039/D1SM00077B.
51. Kharazmi, A.; Priezjev, N.V. Diffusion of a Janus Nanoparticle in an Explicit Solvent: A Molecular Dynamics Simulation Study. *J. Chem. Phys.* **2015**, *142*, 234503, doi:10.1063/1.4922689.
52. Fadda, F.; Matoz-Fernandez, D.A.; Van Roij, R.; Jabbari-Farouji, S. The Interplay between Chemo-Phoretic Interactions and Crowding in Active Colloids. *Soft Matter* **2023**, *19*, 2297–2310, doi:10.1039/D2SM00957A.

 doi:10.20944/preprints202409.0820.v1

53. Howse, J.R.; Jones, R.A.L.; Ryan, A.J.; Gough, T.; Vafabakhsh, R.; Golestanian, R. Self-Motile Colloidal Particles: From Directed Propulsion to Random Walk. *Phys. Rev. Lett.* **2007**, *99*, 048102, doi:10.1103/PhysRevLett.99.048102.
54. Dunderdale, G.; Ebbens, S.; Fairclough, P.; Howse, J. Importance of Particle Tracking and Calculating the Mean-Squared Displacement in Distinguishing Nanopropulsion from Other Processes. *Langmuir* **2012**, *28*, 10997–11006, doi:10.1021/la301370y.